First mirror erosion–deposition studies in JET using an ITER-like mirror test assembly

OPEN ACCESS
IOP Publishing | International Atomic Energy Agency Nuclear Fusion

Nucl. Fusion 61 (2021) 046022 (13pp) https://doi.org/10.1088/1741-4326/abdb92

First mirror erosion–deposition studies in JET using an ITER-like mirror test assembly

M. Rubel[1,*], Sunwoo Moon[1], P. Petersson[1], A. Widdowson[2], R.A. Pitts[3], S. Aleiferis[4], E. Fortuna-Zaleśna[5], G. De Temmerman[3] and R. Reichle[3]

[1] KTH Royal Institute of Technology, EECS, Fusion Plasma Physics, 100 44 Stockholm, Sweden
[2] Culham Science Centre, Abingdon, OX14 3DB Oxfordshire, United Kingdom of Great Britain and Northern Ireland
[3] ITER Organization, Route de Vinon, CS 90 046, 13067 Saint Paul Lez Durance, France
[4] Institute of Nuclear and Radiological Sciences and Technology, Energy and Safety, National Center for Scientific Research 'Demokritos', Athens, 15310, Greece
[5] Warsaw University of Technology, 02-507 Warsaw, Poland

E-mail: Marek.Rubel@ee.kth.se

Received 10 November 2020, revised 31 December 2020
Accepted for publication 13 January 2021
Published 15 March 2021

Abstract

Mirror tests for ITER have been carried out in JET for over 15 years. During the third JET campaign with the ITER-like wall (2015–2016), comprising a total tokamak plasma exposure duration of 23.4 h and 1027 h of glow discharge cleaning, a new experiment was performed with a specially designed ITER-like test assembly housing six polycrystalline molybdenum mirror samples and featuring trapezoidal entrance apertures simulating the geometry of cut-outs in the diagnostic first wall of the ITER shielding blanket. The assembly was installed on the vacuum vessel wall at the outer midplane, set back radially behind the JET poloidal outer limiters such that the contact with thermal plasma should be largely avoided. The total and diffuse reflectivity of all mirrors was measured in the range 300–2500 nm before and after exposure. Post-exposure studies of mirror surface composition and of surfaces outside and inside the assembly were performed using microscopy, x-ray spectroscopy and ion beam analysis methods. The main results are: (i) no measured degradation of total reflectivity; (ii) diffuse reflectivity increased especially at short wavelengths (below 500 nm) from 1.1 to 2.7% and from 0.8%–1.3% above 1000 nm; (iii) mirrors were coated with a thin co-deposited layer (∼20–30 nm) containing carbon, oxygen and traces of nitrogen, beryllium and metals (Ni, Cr, Fe); (iv) no deuterium was detected; (v) surface composition of the mirror box inner walls was similar to that of the mirrors; (vi) $\lesssim$100 nm thick beryllium was the main component on external surfaces of the assembly. These results provide new input to ITER both for the modelling of FM erosion/deposition and for the consideration of requirements for mirror cleaning methods.

Keywords: JET tokamak, first mirror test, plasma diagnosis, erosion–deposition, ITER

(Some figures may appear in colour only in the online journal)

[*] Author to whom any correspondence should be addressed.

1. Introduction

Metallic first mirrors (FM) are essential components of many plasma-viewing diagnostic systems on ITER. Transmission of light signals will rely on mirrors which are the first elements of periscope-shaped systems to guide the light through the shielding blanket. According to the current plan there will be about 80 FM in ITER [1]. A critical issue is the potential modification of the FM reflectivity due to erosion–deposition processes during operations, with the majority of any deposited material expected to be beryllium (Be) eroded from the first wall panels which cover ∼95% of the main chamber surface.

Predicting the amount of erosion or deposition on mirror surfaces is a complex task with many unknowns and uncertainties. For example, simulations performed with the so-called Monte-Carlo-mirror code for the motional Stark effect diagnostic predicted the deposition of a Be layer on the first mirror at the rate of about 200 nm in one year of ITER operations [2]. In contrast, recently performed Monte-Carlo simulations of erosion–deposition on the ITER port plug surfaces have shown that most mirrors in the main chamber would be under erosion-dominated conditions, despite rather high gross Be deposition rates (up to 0.1 nm s^{-1}) [3]. These simulations took into account the neutral particle transport in a prescribed and fixed plasma background. Extrapolations of the plasma parameters were performed based on experimental observations, scaling and previous results from plasma fluid simulations of the ITER edge plasma. Building on these flux estimates, a study was performed for the FM of the H_α main chamber spectroscopy system using the Zemax OpticStudio software [4]. It was concluded that most of the mirror surface would be under net erosion conditions, while deposition would occur only on the mirror edges. It should be mentioned that this work used a simplified approach to erosion and deposition, with an average particle energy instead of the complete energy distribution, and a uniform distribution at the entrance of the cut-out in the blanket. In the face of the large uncertainties and spread in results of the numerical simulations, experiments are critical to understand the underlying physics.

Mirror tests have been carried out in several devices [5–8]. The JET first mirror test (FMT) programme for ITER started in 2002 with planning of mirror location, the design of test specimens and mirror carriers [5]. To date, exposures during five separate campaigns have been performed, with the first taking place during the 2005–2007 campaign in the presence of carbon plasma-facing components (PFCs), i.e. in JET-C [9, 10]. This was followed by another exposure, also in the JET-C environment [11], and then three more in JET with the ITER-like wall (JET-ILW) configuration [12–14] composed of (mostly) Be PFCs on the chamber wall and tungsten in the divertor [15, 16]. During these five campaigns over 100 mirror samples were tested. The exposures were performed using holders of a straight 'pan-pipe' geometry in which cubic specimens (1 cm^3) were located in narrow cavities (i.e. channels) at various distances with respect to plasma, thus resulting in different solid angle for particle bombardment [5]. The tests in the ILW configuration found consistently that mirrors in the divertor region suffered severe reflectivity loss caused by deposition, whilst those in the main chamber maintained good optical performance. During the exposures, mirror samples installed on the main chamber wall (in both JET-C campaigns and the first ILW campaign (ILW-1) were housed in two types of the holders: with and without a magnetic shutter to protect against wall conditioning processes [principally glow discharge cleaning (GDC)] [5]. No difference in surface morphology was found between the shutter-protected and unprotected mirrors exposed during ILW-1 [12].

The geometry of the exposure arrangement in the FMT programme was quite different from the planned ITER situation, which uses primarily pinhole type constructions with large opening apertures in the ITER diagnostic first wall (DFW). Good examples are the Visible and IR viewing and other spectroscopic diagnostics e.g. divertor impurity monitor and H-alpha monitor [17]. Therefore, to extend the scope of studies and to investigate the role of the opening geometry, a new experiment was performed in JET throughout the third ILW campaign (ILW-3): a specially designed, fully remote handling (RH) compatible ITER-like mirror test assembly (ILMTA) housing six mirror samples was exposed on the outside midplane main chamber wall. A technical description of this Inconel 718 assembly, material selection, production method using additive manufacture process, and pre-installation analyses (thermal, electromagnetic) can be found in [18]. The aim of this paper is to provide a comprehensive report on optical mirror properties and surface morphology of the exposed mirrors (and also of the internal and external walls of the ILMTA), together with an analysis of the results.

2. Experimental

Six polycrystalline molybdenum (Mo) mirror samples were exposed. The material choice was justified by the fact that the same type of samples has been used in all stages of the FMT programme, thus enabling direct post-exposure comparison. As shown by the compilation of images in figure 1, the system notably comprises trapezoidally shaped openings to simulate the design of FM apertures in the ITER DFW. The Inconel 718 assembly is mounted on the JET outboard midplane wall, toroidally located between one of the outer poloidal limiters (OPL) and the lower hybrid launcher, figures 1(*a*) and (*b*). In JET the default direction of the toroidal field and plasma current is always 'clockwise' looking from the top of the machine; the red arrow in figure 1(*a*) marks the toroidal field direction. In the assembly interior, three holders, each carrying a pair of samples (shaded in blue in figure 1(*c*), with the mirror sample numbers identified) and marked A, B and C are located respectively in the line-of-sight (LoS) of the pinholes of the trapezoidal entrance apertures A, B and the aperture C, which is a simple orifice without 'ITER-like' geometrical structure. Figure 1(*d*) provides a view of the rear side of one of the sample holders. The holders are composed of two parts, with the E-shaped inner wall structure thus forming together two channels for the installation of mirror samples. The outer wall is L-shaped with screw holes in the horizontal part for attaching the holder to the ILMTA, as indicated by the arrow in figure 1(*d*). The mirror surfaces are inside the assembly, while their rear

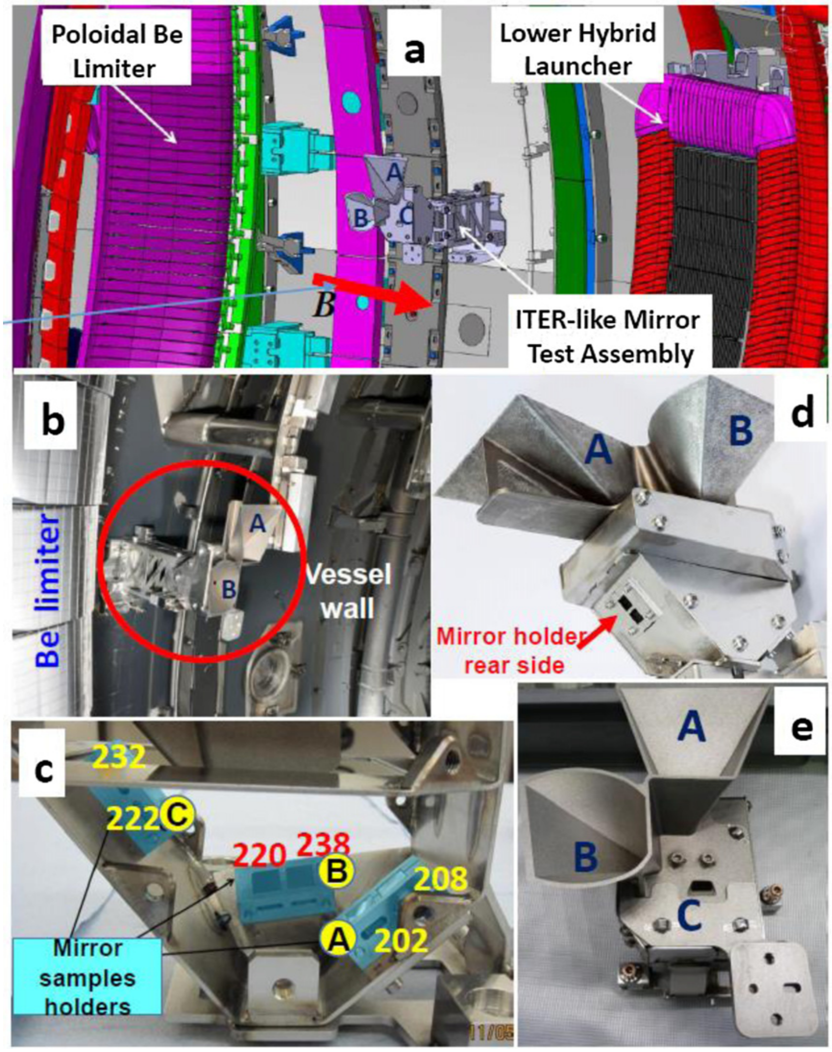

Figure 1. ITER-like test assembly for mirror test in JET: (*a*) the JET wall map with the assembly and nearby structures; a red arrow marks the magnetic field (*B*) direction; (*b*) complete unit installed on the JET vacuum vessel wall; (*c*) interior of the box with three mirror holders-A, B and C—marked in dark blue and the numbers of respective mirror samples; (*d*) side view of the assembly; (*e*) assembly from the plasma-facing perspective with the location of three apertures (A–C) to their respective mirror holders.

sides directly face the tokamak environment in the scrape-off layer. No 'control' mirror samples or material markers, located away from the optical entrance pinholes were included in the assembly.

As seen in figure 1(*a*), aperture opening A is directed upwards towards the top of the JET chamber, aperture B points towards the neighbouring OPL in the anticlockwise direction looking from the top of the machine (thus in the opposite direction to the JET standard plasma current and toroidal magnetic field), whilst aperture C (without trapezoidal opening) views the lower part of the chamber. The viewing directions were chosen to approximate the range of those which will be employed by diagnostics using FMs on ITER, with opening B specifically intended to match situations on ITER with tangentially viewing LoS passing close to Be first wall panels located on each side of ITER port plugs housing the DFW in which the opening apertures are embedded.

The distance between the last closed flux surface (LCFS) for outer wall limited plasmas (and thus the innermost OPL radius) and the radially innermost edge of the ILMTA was 10 cm, matching the recess distance of the DFW from the innermost first wall radius of ITER. The mirror holders (and mirror surfaces) were located 13–15 cm deeper, i.e. 23–25 cm away from the LCFS. For comparison, this distance is at least 17 cm shorter than for mirrors exposed in cassettes used for the FMT programme when the closest mirror was 42 cm behind the LCFS [9].

The exposure was performed during the third ILW campaign (2015–2016) comprising in total 4416 pulses (shot range: #88089–82504), 23.4 h of plasma with 18.5 h of X-point operation, 15.4 h in L-mode and 8.0 h in H-mode. The total input energy was 245 GJ corresponding to an average input power of 2.9 MW; a distribution of input power versus the operation time under given conditions is presented in figure 2, while a histogram in figure 3(*a*) shows the temporal distribution of plasma in contact with respective tiles of the OPLs which occurs mainly during the start-up phase, but occupies only about 20% of the total plasma time. As addressed

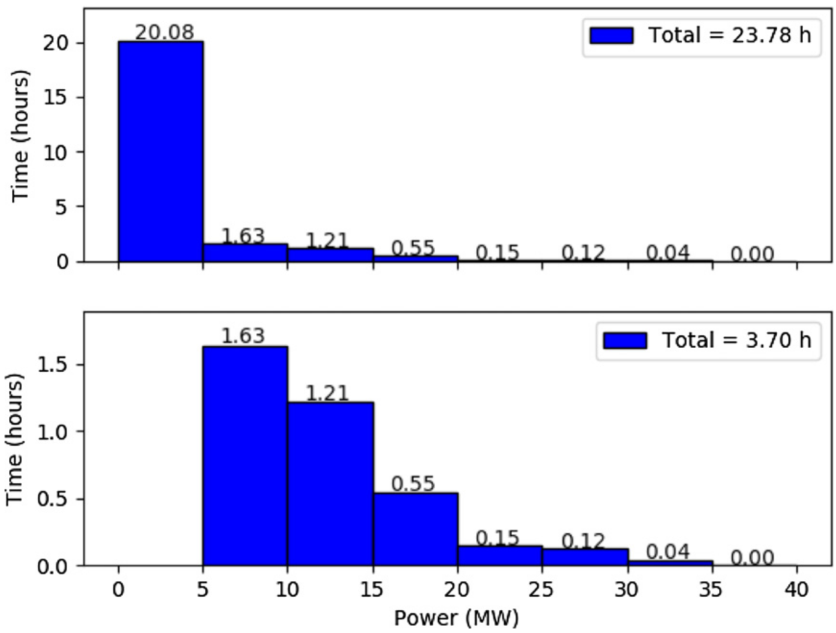

Figure 2. Time at different input power levels throughout the ILMTA exposure in ILW-3. Upper figure includes all input power. Lower figure excludes data where input power is below 5 MW.

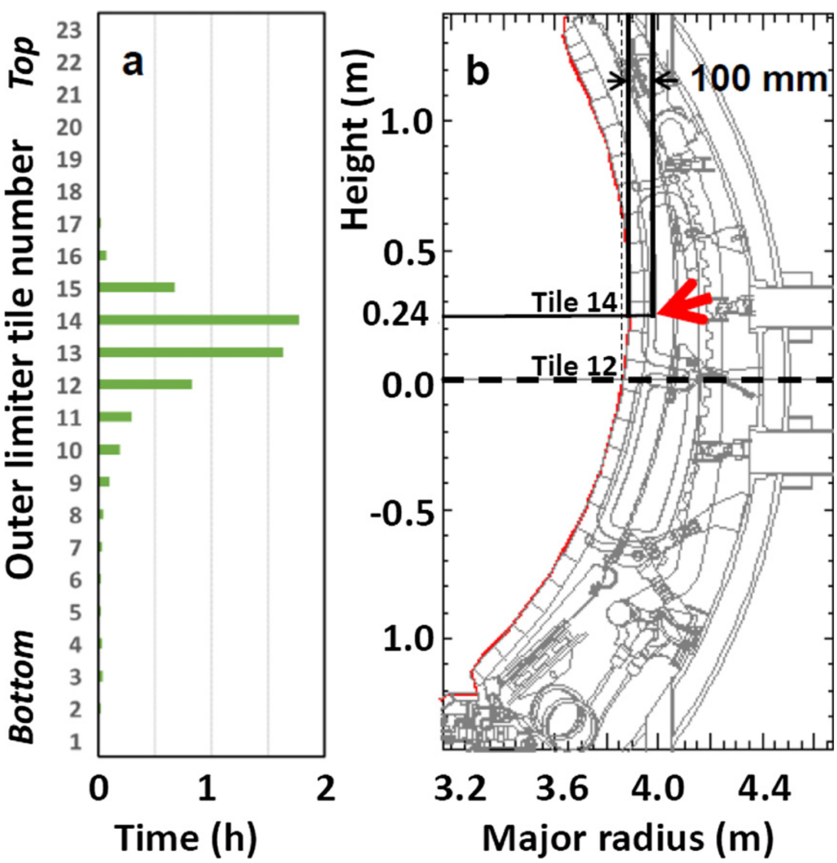

Figure 3. (*a*) Distribution of limiter plasma position and time within 2 mm of the outer limiter surfaces; (*b*) poloidal cross section of the outer wall with a marked position of the ITER-like test assembly.

in [19], it is clear that the interaction occurs mainly at the midplane, particularly with tiles 12–15, i.e. in the poloidal vicinity of the mirror assembly, as shown in figure 3(*b*). The assembly location is marked with an arrow.

Figure 4 gives the distribution of time spent at a given separation between the plasma separatrix (diverted phases) or LCFS (limiter phases) and the innermost radial location of the OPLs at the outside midplane. The ILMTA surface is recessed

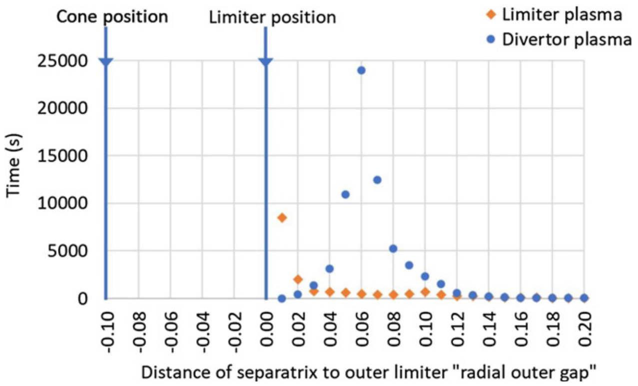

Figure 4. Distribution of time spent at given separatrix/LCFS location with respect to the innermost radial position of the OPL at the outside midplane. The mirror cone surface is recessed 10 cm behind the outer limiter.

10 cm behind the outer limiter. For the vast majority (96%) of limiter plasma time (a total of 16 400 s), the LCFS is within 20 cm of the OPL, and within 2 cm for 64% (10 500 s) of the time. Given the errors in the magnetic equilibrium reconstruction, this 64% corresponds evidently to plasmas limited on the OPLs. For diverted plasma phases, which make up the majority (79%) of the total ILW-3 plasma time, the outboard midplane separatrix is also within 20 cm of the OPL radius, with a clear peak at around 6 cm and FWHM ∼2 cm (not accounting for any error in the absolute position in the separatrix location from the magnetic equilibrium reconstruction).

Unfortunately, the plasma boundary diagnostics at JET do not permit a detailed survey of the plasma background parameters pertinent to the exposure. Such backgrounds are a key feature of any numerical simulations which may be conducted (and which are in fact currently in preparation) to benchmark against this ILMTA exposure. They must instead be generated through dedicated plasma simulations, an exercise which has already been conducted in the framework, for example, of Be migration studies on JET [20].

A very important aspect of this ITER-like mirror exposure experiment is the fact that, owing to design restrictions, it was not possible to incorporate mechanical shutters in front of the entrance pinholes (as had been the case in some of the earlier FMT exposures). As a consequence, the mirror test samples were also exposed to all periods of GDC in deuterium, performed as standard on JET before every campaign following a vessel opening. A total of 1027 h [14] of GDC with a gas feed of 1.5 Pa m^3 s^{-1} [21, 22], were performed during the period in which the ILMTA was present in the torus. It is stressed that mirror samples exposed during the same ILW campaign within the FMT programme were also unprotected by a shutter [14], thus making it possible to compare results for samples from the two systems after the exposure.

Before and after ILMTA exposure, the total and diffuse reflectivities of all mirror samples were measured in the range of 300–2500 nm using a dual-beam spectrophotometer, Lambda 950, Perkin Elmer. Post-exposure studies comprised microscopy: atomic force (AFM) and scanning electron (SEM) combined with energy dispersive x-ray spectroscopy (EDX). Quantitative depth profiling of surface species using a gas ionization detector [23] for time-of-flight heavy ion elastic recoil detection (ToF-HIERDA) with a 36 MeV ^{127}I^{8+} beam was performed both on the mirrors and on several internal and external surfaces of the assembly plates. The technique has depth resolution of 10–15 nm, while the lateral resolution is poor due to the beam-to-surface grazing angle of 22.5° and the resultant beam spot area of 1 × 3 mm^2.

Unexposed mirrors, produced in the same way as those used in the ILMTA and FMT programme, were analysed with SEM, EDX and HIERDA. The structures of the trapezoidal ILMTA openings were examined only visually because their shape (complex geometry) and size made it impossible to insert the components into any chamber of the surface analysis stations and it was decided not to physically cut the apertures in order to preserve the assembly for possible future exposures.

3. Results and discussion

3.1. Reflectivity

Visual inspection of the mirrors and plasma-facing trapezoidal structures after exposure once the ILMTA was extracted from the machine did not indicate any noticeable surface features suggesting significant erosion and deposition. The series of graphs in figure 5 show the initial and post-exposure reflectivity characteristics for one mirror from the pair in each of the three mirror holders. Plots for the total reflectivity are given in figures 5(a)–(c), while the diffuse reflectivity and its average change (in percent) following the exposure are shown in figures 5(a′)–(c'). These results are representative for all six mirrors. For comparison, reference data [5, 24] for the total reflectivity of a Mo mirror are also plotted; the diffuse component of freshly produced mirrors is in the range 0.5%–1.2%.

Average relative changes in the total reflectivity, $R(t)$, and the diffuse component, $R(d)$, are compiled in table 1. The change is defined as the ratio, for respective wavelength, of the difference between the post-exposure and initial reflectivity divided by the initial reflectivity: $[\boldsymbol{R}_{\mathbf{exp}} - \boldsymbol{R}_{\mathbf{initial}}] / \boldsymbol{R}_{\mathbf{initial}}$. The main result is that the total reflectivity has not been degraded. On the contrary, there is a small positive change in the range 300–2500 nm: 0.6%–2.0% on average. Below 1000 nm the performance is slightly improved by 2%–7% relative to the initial values. The improved reflectivity is probably related to at least partial removal of molybdenum surface oxides (Mo_x) under the exposure to a hydrogen (deuterium)-rich atmosphere at elevated temperature; at all times mirrors were at the JET vacuum vessel wall temperature, i.e. 160 °C –220 °C. It may be supposed, in fact, that the actual reflectivity during the exposure in the hydrogen-rich atmosphere of JET was even greater than shown in plots of figures 5(a)–(c), but then was decreased again due to the oxide formation after retrieval of the samples from JET. The formation of oxides on Mo surfaces exposed to air is unavoidable [25–27], and their presence on mirrors from JET-ILW was discussed in [12], where the thickness was determined at around 10 nm. It should be stressed that the minimum time between the vacuum vessel vent prior to shutdown and

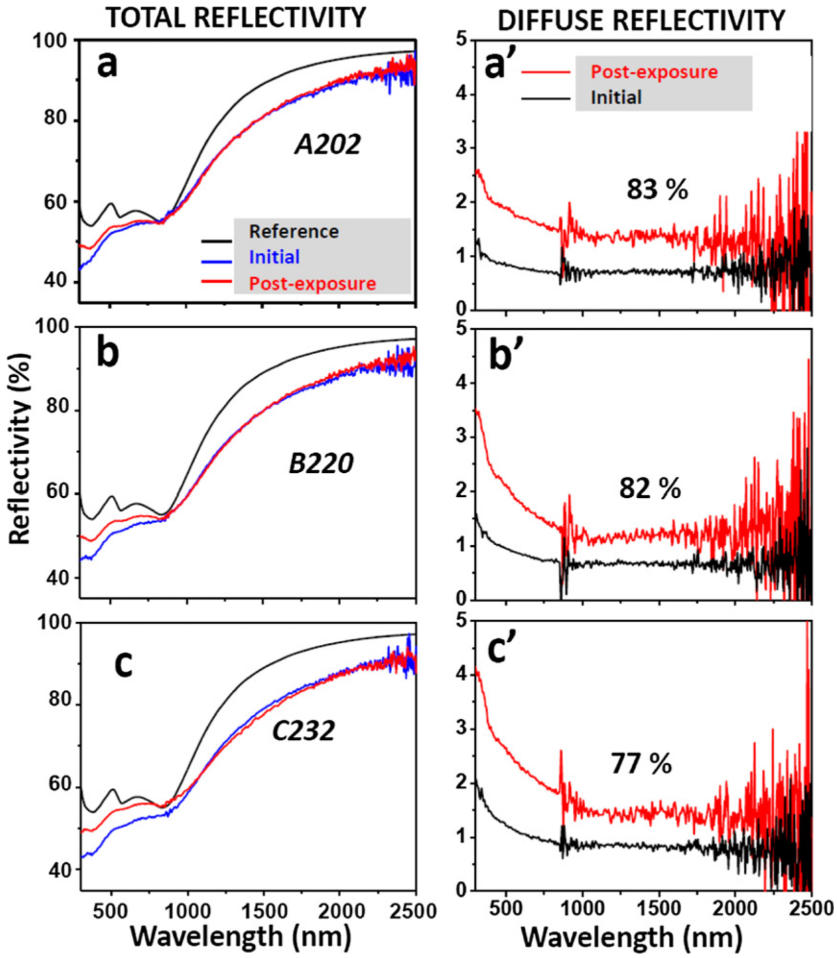

Figure 5. Total and diffuse reflectivity of three mirrors (one from each holder) before and after the exposure. The relative post-exposure increase of diffuse reflectivity is given in respective frames.

Table 1. The average change of mirror reflectivity after exposure with respect to the initial values.

	$R(t)$ change (%)		
Mirror	Range: 300–2500 nm	Range: <1000 nm	$R(d)$ change (%)
A202	1.0	2.2	83
A208	0.7	2.4	70
B220	1.6	4.2	82
B238	0.6	5.2	64
C232	2.0	7.7	77
C222	1.0	5.2	71

ex-situ measurements is several months (the air flow through JET is 5000 m^3 h^{-1} during venting [28]). The presence of oxygen on mirrors prior to and after exposure to plasma will be discussed further in section 3.2.1.

Quite significant in relative terms are the changes of the diffuse reflectivity, especially in the short wavelength range below 500–700 nm: from 1.5%–2.0% to 2.8%–4.0%. Above that range, an increase from 0.8% to 1.3% is measured. The relative increase of diffuse reflectivity is shown in figures 5(a')–(c'). Determined by AFM on the exposed surfaces, the average roughness was 3.3–4.0 nm.

3.2. Surface composition

3.2.1. Mirrors. The initial, as-manufactured, to mirror surfaces contained some imperfections, especially small cavities most probably related to the production of polycrystalline Mo involving powder technology. Using EDX, some traces of oxygen and carbon are detected on the Mo surface. Results for the exposed mirrors are shown in figures 6 and 7: electron micrographs and EDX spectra of local analysis. Certain surface imperfections such as cavities and dust particles are observed. Spectra recorded on the dust-free mirror surface (e.g. spot 4 in figure 6) show only the presence of Mo and a small oxygen feature, ∼10% atomic, while only carbon has been detected in all other particles shown in figure 6, i.e. the EDX spectrum for spot 1 may be taken as typical.

Micrometer-size grains containing carbon only suggest a residue of the diamond polishing paste. In other areas, silicon (Si) and aluminium (Al) particles (but not Si and Al occurring together) were detected. The Al presence can be associated with the contamination caused by the RH equipment made of Al used for all in-vessel operations during JET shut-downs. The issue of dust generation by RH has been addressed in detail in [28].

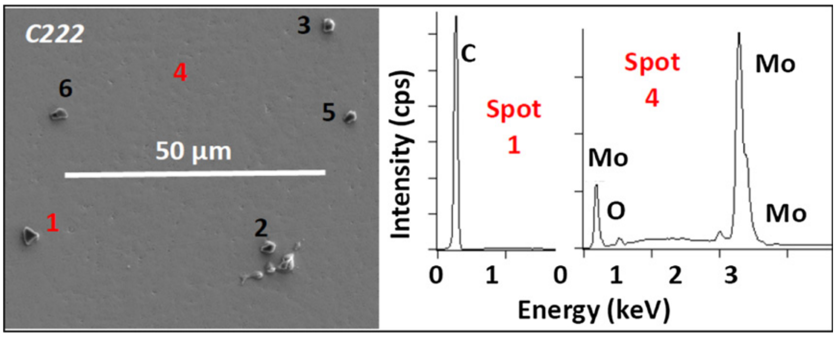

Figure 6. Surface topography of mirror C222 and EDX spectra recorded at several spots. Spectrum for Spot 1 is representative for spots 2, 3, 5 and 6.

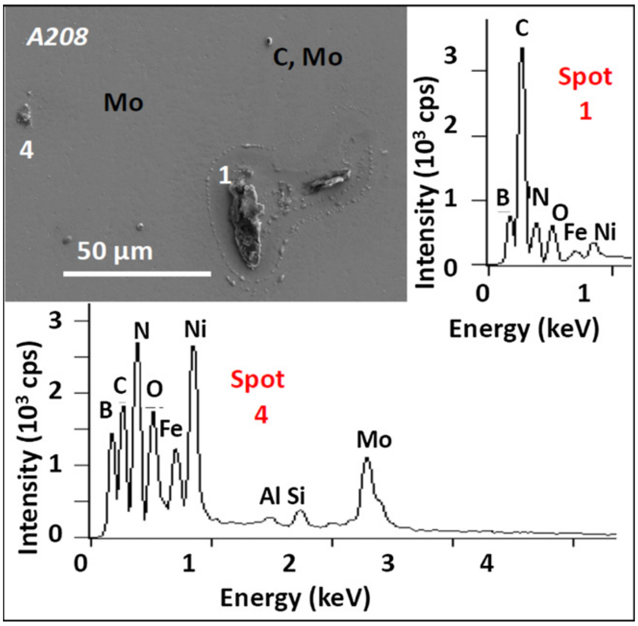

Figure 7. Surface topography of mirror A208 and EDX spectra recorded on dust particles of complex composition.

The SEM images and EDX spectra in figure 7 prove the existence of a complex composition for some surface particulates, comprising both low-Z and medium-Z elements occurring together (B, C, N, O, Al, Si, Fe, Ni), suggesting their formation in the tokamak vessel. The presence of boron (B) accompanied by a significant nitrogen (N) feature, may suggest a contribution from boron nitride (BN) which can be related both to a lubricant used in the RH equipment and residual dust remaining in the vessel following the catastrophic crash of the BN head of the fast reciprocating probe diagnostic during the ILW-2 campaign; the probe has never since been reinstalled in JET. No Be-containing particulates have been identified by EDX, though this does not exclude the presence of Be since the latter is very difficult to detect in mixed materials due to the strong attenuation of low energy x-rays (K_α(Be) = 108 eV). The results in figure 7 thus suggest long distance transport of dust particles to areas shadowed from direct plasma impact, as also reported for the FTM programme samples from the main wall and the divertor [14, 24, 29].

Figure 8 compiles HIERDA depth profiles of species present on surfaces of a selection of the exposed mirror samples: two from holder A and single samples from holders B and C. Table 2 collects the atomic concentrations of the respective species. For comparison, table 2 also includes results for two types of unexposed mirrors (freshly polished and after long-term storage in plastic bags) and for the FMT programme specimens exposed during the ILW-3 campaign on the main chamber wall in the adjacent octant of JET to the location of the ILMTA. There was no shutter on the cassette housing the mirrors samples of the FMT programme.

Unexposed mirrors are coated with a thin layer (not exceeding 10 nm) containing O and C impurity species and their amount increases in time when mirrors are stored; the layer thickness increases to around 15 nm. All exposed Mo surfaces are modified by erosion and deposition processes resulting in the formation of thin layers containing a mixture of Inconel components (Ni, Cr, Fe) and light elements (H, C, N, O). The majority of species is in a layer of thickness <20–30 nm. The extension of profiles to a greater depth is most probably connected with the deposition in surface imperfections, i.e. in cavities, seen in figures 6 and 7, acting as tiny shadowed areas. The impact of shallow implantation and diffusion on the recorded profiles cannot be fully excluded taking into account the long-term mirror exposure at elevated temperature in an environment containing energetic particles, both neutrals and ions (the latter only possible in the ILMTA cavity during GDC).

Faint features of the deposited elements in HIERDA spectra shown in figure 9 for two of the mirrors clearly prove that all impurity species (elements) occur in very small quantities only in the very surface layer. The exact layer thickness (better than given above) cannot be determined since the depth resolution of the technique is on the level of 10–15 nm. There is no deuterium in the layer (lower detection limit for D is 1×10^{15} cm^{-2}), whereas Be in quantities above the detection limit ($\sim 5 \times 10^{14}$ cm^{-2}) has been identified only on two mirrors from two different holders: B and C. The presence of medium-Z metals is most probably connected with sputtering of the Inconel trapezoidal opening apertures by charge-exchange neutrals (CXN) during tokamak plasma exposure, or by energetic ions (several 100 eV) during GDC. The absence of shutters in the ILMTA (see above) prevents a distinction being

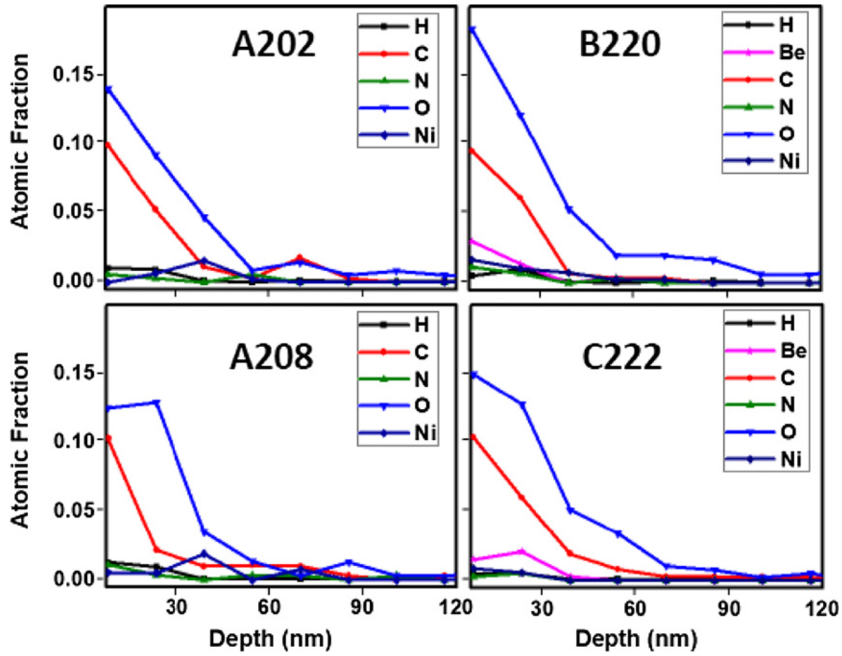

Figure 8. ToF-HIERDA depth profiles of species on mirror sample surfaces from different holders.

Table 2. Surface composition of mirrors from the ILMTA, unexposed reference specimens and exposed in ILW-3 within the FMT programme running in parallel with the ILMTA exposure. All concentrations in 10^{15} cm^{-2}.

Mirror	H	D	Be	C	N	O	Ni + Cr + Fe
A202	2.2	—	—	18.4	1.4	30.2	2.5
A208	2.4	—	—	14.5	1.8	30.2	3.0
B220	1.6	—	4.8	16.8	2.2	38.0	3.7
B238	1.1	—	—	20.8	0.4	39.3	2.2
C222	1.3	—	3.9	19.1	0.8	36.3	1.5
C232	1.4	—	—	19.0	1.9	27.9	1.6
Initial freshly polished	Traces	—	—	3	—	7	—
Initial long-term storage	Traces	—		5		10	
Mirrors from FMT, ILW-3 [14]	Not determined	Traces	0–2.0	11–20	2–7	5–19	0–2

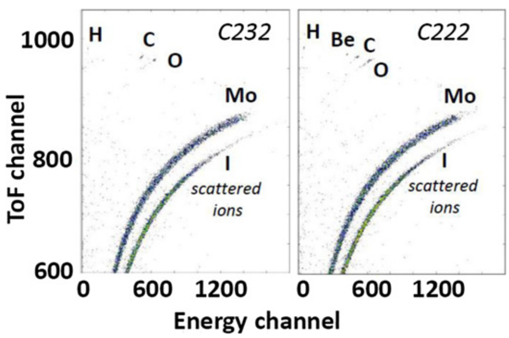

Figure 9. ToF-HIERDA spectra proving the presence of co-deposited species in minute quantities on the mirror sample surfaces and only in the very surface layer.

made between the contributions of these two components, as it does for all other features revealed by the surface analysis. Some sputtered atoms enter the assembly interior through the apertures.

Be originates from the erosion of ILW limiters or other Be PFCs in the main chamber (e.g. the upper dump tiles at the top of the vacuum vessel), while N neutrals penetrate into the box in connection with gas puffing (extrinsic seeding) for plasma edge cooling. It is important to stress that N has been detected on surfaces of all materials retrieved from JET-ILW and studied with HIERDA and EDX [12, 14, 30–32]. It is a result of co-deposition/co-implantation of plasma species and not related to the N_2 adsorption from air during the sample exposure to ambient atmosphere since the amounts which can be adsorbed from air exposure are below the HIERDA detection limits. Retention of N in wall materials has been confirmed in dedicated experiments with N_2 puffing [33] and also using the tracer $^{15}N_2$ in JET and in other machines [34–36]. Though a definite statement on the origin of carbon is not possible, it may be assumed to originate from several sources: (i) C atoms or hydrocarbon neutrals from the plasma; (ii) the aforementioned presence of residual diamond grains used for polishing; (iii) a trace constituent of the assembly materials.

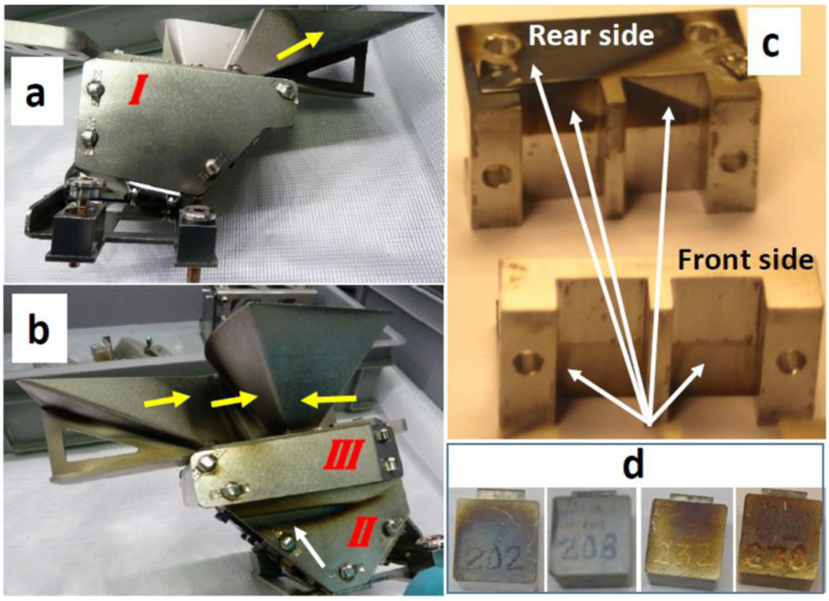

Figure 10. Appearance of a selection of exposed surfaces of the ILMTA: (*a*) and (*b*) the assembly shown from two sides; (*c*) two parts of the mirror holder with deposits on the rear side; (*d*) deposits on the rear sides of the mirrors.

Results obtained for the two sets of mirrors (housed in the ILMTA and cassettes of the FMT programme [14]) exposed to plasma on the main chamber wall during ILW-3 are nearly identical. In both cases total reflectivity was retained, diffuse reflectivity increased from 1%–1.5% to 2.5%–4%, surfaces are coated with thin films and the surface compositions are nearly identical. The only difference is in the oxygen level which reaches somewhat greater values on specimens from the ILMTA.

To summarize the key findings of this section, it is stressed that the optical properties of mirrors exposed inside the special ILMTA are similar to those of the reference, unexposed samples. In the short wavelength range the properties are even somewhat improved, despite the modification of the surface composition by deposited or co-implanted species. It is impossible, however, to say whether and what kind of dynamic changes to the surface state may have occurred during the exposure. The amounts of dust and trace deposition of elements found on the sample surfaces had no negative impact on the mirror performance.

3.2.2. Walls of the assembly. The photographs in figures 10(*a*) and (*b*) show the external surfaces of the assembly after exposure. In comparison to figures 1(*d*) and (*e*), prior to the installation in JET there is clear discoloration of the plates marked I–III: a fairly uniformly distributed brownish deposit and only one distinct deposition zone marked with an arrow on plate II. These particular plates have been singled out here since they are easily dismountable units with dimensions amenable to surface analysis. The trapezoidal apertures, however, are part of the main additive manufactured assembly and could not be analysed without cutting the assembly. As explained earlier, this was not performed in the interests of maintaining the integrity of the assembly for potential use in further JET campaigns. Similar 'distinct' regions of deposition can also be found on the external surfaces [marked with arrows in figures 10 (*a*) and (*b*)] of the trapezoidal openings, but the inside surfaces are more uniformly discoloured, with no obvious strong deposition. As shown in figures 10(*c*) and (*d*), clear deposition patterns have been formed on the rear side of the mirror holder, inside the channels behind the mirrors (all areas are marked with arrows) and on the rear side of the mirrors.

Internal and external surfaces of the three plates identified in figure 10, as well as the rear side of the mirror holders, were examined with ToF-HIERDA, which is particularly suited to this analysis due to high compositional sensitivity and selectivity of the system employed in the studies [23]. Figure 11 compiles further images of the internal and external surfaces of the plates, where the positions of the analysed points 1–17 are marked. In general, there is no visible deposit on the internal surfaces, with the exception of some narrow blackish deposits which may be seen at the edges in the internal areas which were in fact exposed externally due to some imperfections in mounting the plates. Particular areas on plate III are marked in figure 11, with the X identifying point 14 on the edge deposit analysed with HIERDA. A full account of the surface composition on plates is given in tables 3–5.

The data show clearly that the surfaces inside the box remained fairly clean, with only trace amounts of light species: Be, C, N and O. The composition matches that detected on the mirrors. This is a surprising finding of the study and is not easy to explain. There is no *a priori* reason why it should be the case that the mirror surfaces, exposed directly to incoming fluxes from plasma/GDC exposure, should bear similar coating thickness and composition as the rest of the interior surfaces. One possibility is the presence of some kind of parasitic

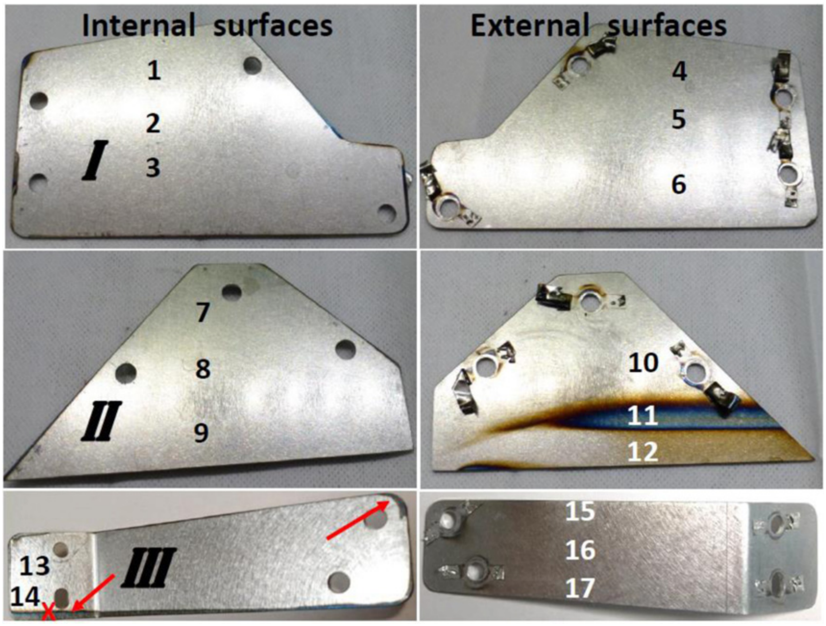

Figure 11. Internal and external surfaces of plates I–III of the assembly. Analysed points 1–17 are indicated. On plate III the deposition areas are indicated with arrows and the exact position of the analysis spot is marked by an X.

Table 3. Surface composition of internal and external walls of plate I (see figures 10 and 11). All concentrations in 10^{15} cm^{-2}.

Point	H	D	Be	B	C	N	O	W
				Inside				
1	3	—	3	10	6	11	34	—
2	2	—	3	2	5	5	33	—
3	2	—	2	—	4	4	28	—
				Outside				
4	3	—	30	—	25	6	60	2
5	2	—	21	—	22	5	48	2
6	3	—	9	—	24	2	30	2

Table 4. Surface composition of internal and external walls of plate II (see figures 10 and 11). All concentrations in 10^{15} cm^{-2}.

Point	H	D	Be	C	N	O	W
			Inside				
7	2	—	1	6	2	39	—
8	2	—	2	7	2	39	—
9	2	—	2	5	4	32	—
			Outside				
10	7	10	121	37	13	91	1
11	51	425	652	69	67	401	5
12	3	145	152	65	18	187	—

Table 5. Surface composition of internal and external walls of plate III (see figures 10 and 11). All concentrations in 10^{15} cm^{-2}.

Point	H	D	Be	B	C	N	O	Na/Mg	Al/Si	W
					Inside					
13	7	—	3	—	12	31	33	—	—	—
14	17	25	261	—	50	28	223	—	—	0.1
					Outside					
15	3	2	118	—	32	9	104	3	6	—
16	3	1	32	—	37	7	68	4	9	—
17	6	7	63	24	22	20	141	9	16	—

Table 6. Deposit on the rear sides of mirror channels (see figure 10). All concentrations in 10^{15} cm^{-2}.

	H	D	Be	C	N	O	W
Average	9	14	181	28	14	189	1.5
Maximum	25	24	280	50	23	259	7.7
Minimum	4	4	69	12	7	82	0.1

discharge within the cavity, possibly due to the use of GDC throughout the campaign. The difficulty of including mechanical shutters on the entrance pinholes to the assembly and the decision not to include reference mirror surfaces inside the cavity (i.e. not directly exposed to incoming fluxes), means that it is impossible to verify this particular conjecture. The fact that the mirror coatings are similar to those found on the inner walls of some of the structures may also be a coincidence. Any layers growing there (by whatever process) could simply be re-eroded preferentially due to bombardment by incoming fluxes and reflection of eroding species off the mirror surface, similar to the findings reported in [37].

Be together with oxygen (most probably as BeO) are the main components of co-deposits on the external surfaces of the box and also inside the channels of the mirror holders in areas behind the mirrors; data for the holders may be found in table 6. Other species, including C, are in quantities not exceeding 7×10^{16} cm^{-2} even in the deposition belt on plate II, i.e. in point 11. There are some differences between the deposit composition on the exterior surfaces of the different plates. For example plate I is nearly free of deposits.

The most important observation is that the total quantity of solid elements at the analysed locations (Be, C) does not exceed 1×10^{18} cm^{-2}, meaning that even the thickest layer in the belt is less than 100 nm. Since the majority of the ILMTA structure is significantly radially recessed behind the neighbouring OPL or LH launcher structures, it is difficult to imagine any significant plasma thermal flux in this region. However, many of the deposition patterns observed are clearly 'optical' in origin and must have arisen as a result of structural shadowing. This implies a contribution from magnetic shadowing of plasma flux, but could only be confirmed by a full 3D field line tracing analysis accounting for the geometry of local structures in this far scrape-off layer region. Such analysis has not been attempted here, particularly in view of the fact that this deposition on external surfaces has no obvious impact on the state of the internal surfaces and in particular on the mirrors. Perhaps a more likely explanation is that the deposition is a simple consequence of plasma CXN impact during tokamak discharges, which will tend to preferentially erode regions in direct view of the plasma, leaving deposits to grow in regions shadowed by the ILMTA structure itself. The question then arises as to the origin of the light Be-dominated coating of the assembly in general. It is stressed that Be evaporation which was frequently carried out in JET-C [38], was not performed in JET-ILW. This may arise directly from deposition due to plasma neutral outfluxes, or during GDC with perhaps a contribution of vapour deposition after disruptive transients, which have been clearly seen in JET in all ILW campaigns to lead to significant melting of Be, especially on dump plates at the top of the vessel, see e.g. [39]. In fact, such deposition regions are a general feature seen on many components located in recessed areas on JET.

The Be/C concentration ratio found in these external deposits is in the range from 3 to 11, with one exception at point 16, where very small quantity (at the low 10^{16} cm^{-2} level) of both species was deposited. Other elements, including W, are present only at the trace level with maximum measured concentration less than 8×10^{15} cm^{-2}. Indeed, at most of the analysed locations, the W content was below the detection limit.

4. Concluding remarks

The key finding of the study reported here is that optical properties (total reflectivity) of mirrors exposed in an ILMTA on JET with the same plasma-facing material combination as on ITER have not been degraded. Their surfaces have been only mildly affected by neutral/ion fluxes and dust particulates penetrating the assembly during exposure to around 23.4 h of tokamak plasma and over 40x that duration (1027 h) of GDC. The findings of this work confirm earlier results obtained during the extensive JET FMT programme [12–14, 24] and document once again that optical properties of mirrors exposed in the outboard midplane region of the JET main chamber wall are not degraded, despite some observed modifications of the mirror sample surface composition.

Results for mirrors from the special ITER-like assembly and for those exposed in the cassettes of FMT programme are nearly identical, within a few times 10^{15} atoms cm^{-2}, demonstrating that exposures with these two different geometries give nearly the same result. This may suggest that: (i) the impact of GDC in the two cases is either the same or is unimportant; (ii) the aperture geometry has no major impact on the fate of the mirror samples; (iii) both factors mentioned above conspire together to give the same overall result. Pure coincidence cannot be fully excluded, but this could only be verified by further experiments.

It is not possible to extrapolate and translate the results directly to ITER because of the difference in fluxes, input energy, operation time etc. The exposure in JET would correspond by divertor operation time to about 170 ITER pulses lasting 400 s. However, assuming H-mode operation, there is an approximate scaling factor of 40 between JET and ITER in terms of divertor ion fluence [40–42], so that the JET exposure would correspond to only $\sim$4 ITER baseline burning plasma discharges when normalized to this metric. Regarding the main chamber neutral wall fluxes, a JET–ITER comparison can only currently be based on modelling since no measurement of this quantity is available on JET. Such modelling (using the SOLPS code) shows that the behaviour (in terms of neutral energy spectra and poloidal distributions) is similar between the two devices [40–42], although the absolute fluxes at any given point on the wall surface will be sensitive to the assumptions made for the far SOL background plasma temperature and density. Simulations for ITER suggest integrated wall neutral fluxes of 3.8×10^{23} s^{-1} [20], corresponding to 4.8 $\times$ 1016 cm^{-2} s^{-1} taking into account $\sim$800 m^2 of total main chamber wall area.

The experiment provides, as intended, new input to ITER both for the modelling of FM erosion/deposition in a geometrical configuration much closer to that which will be employed in the ITER DFW and in the same plasma-facing component material environment. Even though direct extrapolation to ITER is not possible without a modelling step, in which these JET results are tested against the expectations of simulations, the deposits found on the mirror samples do confirm previous FMT programme findings. As such, they reinforce the expectation that ITER FMs may be characterized by mix-material co-deposits (Be, C, Ni, W with fuel species). They may also partly contribute to the consideration of requirements for mirror cleaning methods [43–45].

A further important result of the study is the similarity between coatings found on mirrors and other internal surfaces (not exposed directly to particles penetrating the pinhole apertures) of the ILMTA cavity. Numerical simulations of the exposure taking into account averaged plasma background properties relevant to the exposures and the full 3D geometry of the system, may be the best way to shed light on the observations. In fact, it is precisely for such numerical modelling, required for extrapolation to ITER, that this experiment was in part conceived.

Acknowledgments

This work has been supported by the Swedish Research Council (VR), Grant 2015–04844. Financial support of the tandem accelerator infrastructure by VR-RFI (contract #2017-00646_9) as well as the Swedish Foundation for Strategic Research (SSF) under contract RIF14-005 is gratefully acknowledged. This work has been partly carried out within the framework of an ITER service contract with the ID ITER/SGS/13/4300000956. The views and opinions expressed herein do not necessarily reflect those of the ITER Organization. ITER is the nuclear facility INB 174.

ORCID iDs

M. Rubel https://orcid.org/0000-0001-9901-6296
Sunwoo Moon https://orcid.org/0000-0002-0865-7387
P. Petersson https://orcid.org/0000-0002-9812-9296
A. Widdowson https://orcid.org/0000-0002-6805-8853
R.A. Pitts https://orcid.org/0000-0001-9455-2698
G. De Temmerman https://orcid.org/0000-0002-4173-0961

References

[1] Costley A.E., Sugie T., Vayakis G. and Walker C.I. 2005 Technological challenges of ITER diagnostics *Fusion Eng. Des.* **74** 109

[2] Brooks J.N. and Allain J.P. 2008 Particle deposition and optical response of ITER motional Stark effect diagnostic first mirrors *Nucl. Fusion* **48** 045003

[3] Kotov V. 2016 Engineering estimates of impurity fluxes on the ITER port plugs *Nucl. Fusion* **56** 106027

[4] Orlovskiy I., Andreenko E. and Alekseev A. 2018 Estimation of neutral fluxes on the first mirror of H-alpha diagnostics in ITER *Fusion Eng. Des.* **146** 827–30

[5] Rubel M.J. *et al*(JET-EFDA Contributors) 2006 Mirror test for international thermonuclear experimental reactor at the JET tokamak: an overview of the program *Rev. Sci. Instrum.* **77** 063501

[6] Wienhold P. *et al* 2005 Exposure of metal mirrors in the scrape-off layer of TEXTOR *J. Nucl. Mater.* **337–339** 1116

[7] Lipa M. *et al* 2006 Analyses of metallic first mirror samples after long term plasma exposure in Tore Supra *Fusion Eng. Des.* **81** 221

[8] Litnovsky A. *et al* 2019 Diagnostic mirrors for ITER: research in the frame of international tokamak physics activity *Nucl. Fusion* **59** 066029

[9] Rubel M., De Temmerman G., Sundelin P., Coad J.P., Widdowson A., Hole D., Le Guern F., Stamp M. and Vince J. 2009 An overview of a comprehensive first mirror test for ITER at JET *J. Nucl. Mater.* **390–391** 1066–9

[10] Rubel M., Coad J.P., De Temmerman G., Hakola A., Hole D., Likonen J., Uytdenhouwen I. and Widdowson A. 2010 First mirrors test in JET for ITER: an overview of optical performance and surface morphology *Nucl. Instrum. Methods Phys. Res.* A **623** 818

[11] Rubel M., Ivanova D., Coad J.P., De Temmerman G., Likonen J., Marot L., Schmidt A. and Widdowson A. 2011 Overview of the second stage in the comprehensive mirrors test in JET *Phys. Scr.* **T145** 014070

[12] Ivanova D., Rubel M., Widdowson A., Petersson P., Likonen J., Marot L., Alves E., Garcia-Carrasco A. and Pintsuk G. 2014 An overview of the comprehensive first mirror test in JET with ITER-like wall *Phys. Scr.* **T159** 014011

[13] Garcia-Carrasco A., Petersson P., Rubel M., Widdowson A., Fortuna-Zalesna E., Jachmich S., Brix M. and Marot L. 2017 Plasma impact on diagnostic mirrors in JET *Nucl. Mater. Energy* **12** 506

[14] Moon S., Petersson P., Rubel M., Fortuna-Zalesna E., Widdowson A., Jachmich S., Litnovsky A. and Alves E. 2019 First mirror test in JET for ITER: complete overview after three ILW campaigns *Nucl. Mater. Energy* **19** 59

[15] Matthews G.F. *et al* 2007 Overview of the ITER-like wall project *Phys. Scr.* **T128** 127

[16] Matthews G.F. *et al* 2011 JET ITER-like wall-overview and experimental programme *Phys. Scr.* **T145** 014001

[17] Iwamae A., Sugie T., Ogawa H. and Kusama Y. 2009 Divertor impurity-influx monitor for ITER: spectral throughput measurement on an optical prototype for the upper port and optimization of viewing chords based on computerized tomography *Plasma Fusion Res.* **4** 042

[18] Vizvary Z. *et al* 2017 Engineering design and analysis of an ITER-like first mirror test assembly on JET *Fusion Eng. Des.* **123** 1054

[19] Widdowson A. *et al* 2020 Fuel inventory and material migration of JET main chamber plasma facing components compared over three operational periods *Phys. Scr.* **T171** 014051

[20] Romazanov J. *et al* 2020 First Monte-Carlo modelling of global beryllium migration in ITER using ERO2.0 *Contrib. Plasma Phys.* **60** e201900149

[21] Andrew P. *et al* 1999 Tritium retention and clean-up in JET *Fusion Eng. Des.* **47** 233

[22] Wauters T. *et al* 2020 Wall conditioning in fusion devices with superconducting coils *Plasma Phys. Control. Fusion* **62** 034002

[23] Ström P., Petersson P., Rubel M. and Possnert G. 2016 A combined segmented anode gas ionization chamber and time-of-flight detector for heavy ion elastic recoil detection analysis *Rev. Sci. Instrum.* **87** 103303

[24] Rubel M. *et al* 2017 Metallic mirrors for plasma diagnosis in current and future reactors: tests for ITER and DEMO *Phys. Scr.* **T170** 014061

[25] Floquet N. and Bertrand O. 1991 Superficial oxidation of molybdenum at high pressure and low temperature: RHEED and AES analyses of the molybdenum oxide formation *Surface Science* **251–252** 1044

[26] Schintlmeister A., Martinez H.P., Wilhartitz P. and Netzer F.P. 1998 The low-temperature oxidation of industrial molybdenum surfaces *Proc. World Congress on Powder Metallurgy, Superhard /Refractory Metals* (Granada, Spain, October 1998) pp 526–31 (https://www.tib.eu/en/search/id/BLCP:CN029133291/Low-Temperature-Oxidation-of-Industrial-Molybdenum?cHash=ee53dbe21b7ba2caa81ff4714e26ff45)

[27] Schintlmeister A. and Wilhartitz P. 2001 Protection of molybdenum and molybdenum alloy thin films against low-temperature oxidation *15th Int. Plansee Seminar* (Plansee Holding AG, Reutte, Austria, May 2001) ed G. Kneringer, P. Rödhammer and H. Wildner vol 4 p 211 (https://inis.iaea.org/collection/NCLCollectionStore/_Public/33/060/33060932.pdf)

[28] Rubel M. *et al* 2019 Search for mobilized dust during operations with equipment for remote handling in JET with ITER-like wall *Phys. Scr.* **T171** 014048

[29] Fortuna E. *et al* 2017 Fine metal dust particles on the wall probes from JET with the ITER-Like Wall *Phys. Scr.* **T170** 014038

[30] Petersson P. *et al* 2015 Co-deposited layers in the divertor region of JET-ILW *J. Nucl. Mater.* **463** S814

[31] Fortuna-Zaleśna E. Grzonka J., Rubel M., Garcia-Carrasco A., Widdowson A., Baron-Wiechec A. and Ciupiński L.(JET

Contributors) 2017 Studies of dust from JET with the ITER-like wall: composition and internal structure *Nucl. Mater. Energy* **12** 582

[32] Rubel M. *et al* 2018 Dust generation in tokamaks: overview of beryllium and tungsten dust characterisation in JET with the ITER-like wall *Fusion Eng. Des.* **136** 579

[33] Rubel M., Philipps V., Marot L., Petersson P., Pospieszczyk A. and Schweer B. 2011 Nitrogen and neon retention in plasma-facing materials *J. Nucl. Mater.* **415** S223

[34] Petersson P., Rubel M., Possnert G., Brezinsek S. and Pegourie B. Nuclear reaction and heavy ion ERD analysis of wall materials from controlled fusion devices: deuterium and nitrogen-15 studies 2012 *Nucl. Instrum. Methods Phys. Res. Sect. B Beam Interact. Mater. Atoms* **273** 113

[35] Petersson P., Hakola A., Likonen J., Mayer M., Miettunen J., Neu R., Rohde V. and Rubel M. 2013 Injection of nitrogen-15 tracer into ASDEX-Upgrade: new technique in material migration studies *J. Nucl. Mater.* **438** S616

[36] Petersson P. *et al* 2014 Overview of nitrogen-15 application as a tracer gas for material migration and retention studies in tokamaks *Phys. Scr.* **T159** 014042

[37] De Temmerman G. and Pitts R.A. 2008 Substrate-dependent deposition efficiency on mirrors exposed in the TCV divertor *Fusion Eng. Des.* **83** 30

[38] Peacock A.T. *et al* 1990 Impurity coverage and deuterium inventory of beryllium and carbon first wall components after beryllium operation in JET *J. Nucl. Mater.* **176–177** 326

[39] Jepu I. *et al* 2019 Beryllium melting and erosion on the upper dump plates in JET during three ITER-like wall campaigns *Nucl. Fusion* **59** 086009

[40] Pitts R.A. *et al* 2005 Material erosion and migration in tokamaks *Plasma Phys. Control. Fusion* **47** B303

[41] Pitts R.A. *et al* 2019 Physics asis for the first ITER tungsten divertor *Nucl. Mater. Energy* **20** 100696

[42] De Temmerman G., Hirai T. and Pitts R.A. 2018 The influence of plasma-surface interaction on the performance of tungsten at the ITER divertor vertical targets *Plasma Phys. Control. Fusion* **60** 044018

[43] Wisse M. *et al* 2014 Laser-assisted cleaning of beryllium-containing mirror samples from JET and PISCES-B *Fusion Eng. Des.* **89** 122

[44] Moser L. *et al* (JET Contributors) 2016 Plasma cleaning of beryllium coated mirrors *Phys. Scr.* **T167** 014069

[45] Ben Yala M., Moser L., Steiner R., Butoi B., Dinca P., Petersson P., Marot L. and Meyer E. 2019 Deuterium as a cleaning gas for ITER first mirrors: experimental study on beryllium deposits from laboratory and JET-ILW *Nucl. Fusion* **59** 096027